


Cite this: *CrystEngComm*, 2021, 23, 3230

Received 15th February 2021,  
Accepted 16th March 2021

DOI: 10.1039/d1ce00220a

rsc.li/crystengcomm

# Crystal growth and thermodynamic investigation of $\text{Bi}_2\text{M}^{2+}\text{O}_4$ ( $\text{M} = \text{Pd}, \text{Cu}$ )

Nora Wolff, <sup>a</sup> Detlef Klimm, <sup>b</sup> Klaus Habicht<sup>a,c</sup> and Katharina Fritsch <sup>a</sup>

Phase equilibria that are relevant for the growth of  $\text{Bi}_2\text{MO}_4$  have been studied experimentally, and the ternary phase diagrams of  $\text{Bi}_2\text{O}_3$ – $\text{PdO}_2$ – $\text{Pd}$  and  $\text{Bi}_2\text{O}_3$ – $\text{Cu}_2\text{O}$ – $\text{CuO}$  and its isopleth section  $\text{Bi}_2\text{O}_3$ – $\text{CuO}$  were redetermined. It is shown that every melting and crystallization process is always accompanied by a redox process at the phase boundary and that for both title compounds, the valence of the transition metal is lowered during melting. *Vice versa*, during crystal growth,  $\text{O}_2$  must be transported through the melt to the phase boundary. Based on these new insights provided by our thermodynamic studies,  $\text{Bi}_2\text{CuO}_4$  single crystals with a length of up to 7 cm and a diameter of 6 mm were grown by the OFZ technique to be used for investigations of magnetic, electronic and thermal transport properties. The grown crystals were characterized by powder X-ray diffraction, Laue, magnetization and specific heat measurements.

## 1 Introduction

Over the last decades, transition-metal (M) oxides containing  $\text{MO}_4$  square-planar environments in their structure have attracted interest due to their fascinating structure based electronic and magnetic properties.<sup>1,2</sup> Compared to tetrahedral and octahedral coordination, the square planar geometry is rarely found in transition metal oxides because it is thermodynamically less stable.<sup>1,3</sup> However,  $\text{MO}_4$  square planar coordination is typically encountered in  $d^8$  and  $d^9$  electron configurations, for example in Pd, Pt or Cu-based compositions, where it is favorable for electronic ground states.<sup>1</sup> The structure of  $\text{Bi}_2\text{M}^{2+}\text{O}_4$  ( $\text{M} = \text{Pd}, \text{Cu}$ ) is composed of such  $\text{MO}_4$  units forming staggered chains along the *c*-axis.<sup>2</sup>

In the past few decades,  $\text{Bi}_2\text{CuO}_4$  has been extensively studied and has first come into the focus of the high temperature superconductivity community as a non-superconducting structural relative due to its shared  $\text{CuO}_4$  motifs.<sup>4</sup> Since then, it continues to be of fundamental interest as a low-dimensional  $S = 1/2$  Heisenberg antiferromagnet exhibiting a plethora of intriguing phenomena including controversially discussed low-temperature anisotropic magnetic ground state properties that have been studied by bulk magnetization,<sup>2</sup> Raman,<sup>5</sup> antiferromagnetic resonance<sup>6</sup> or neutron scattering techniques,<sup>7</sup>

the observation of magnetically-induced ferroelectricity,<sup>8</sup> and a recent prediction of the realization of a topologically non-trivial double-Dirac metal in  $\text{Bi}_2\text{CuO}_4$  under pressure.<sup>9</sup> In addition,  $\text{Bi}_2\text{CuO}_4$  has recently been investigated as a photocathode material for photoelectrochemical water splitting<sup>10,11</sup> or even for gas-sensing applications.<sup>12</sup>

The isostructural system  $\text{Bi}_2\text{PdO}_4$  has also recently attracted attention following experimental and theoretical work on the thermoelectric properties of similar oxide materials with square planar  $\text{PdO}_4$  units.<sup>13,14</sup> Theoretical work by He *et al.*<sup>15</sup> proposed favorable thermoelectric properties of  $\text{Bi}_2\text{PdO}_4$  arising from a combination of its peculiar electronic band structure mainly related to the involved  $\text{Pd}^{2+}$   $d_{z^2}$  orbitals and a low lattice thermal conductivity. The latter has been ascribed to the presence of heavy  $\text{Bi}^{3+}$  ions in the crystal structure whose  $6s^2$  electron lone pairs are thought responsible for contributing to additional phonon scattering and anharmonic effects.

The tetragonal  $P4/ncc$  crystal structure of  $\text{Bi}_2\text{MO}_4$ , which is shown in Fig. 1, consists of square-planar  $\text{MO}_4$  units and asymmetrically distorted  $\text{BiO}_6$  octahedra.<sup>15,16</sup> The  $\text{MO}_4$  units are stacked along the *c*-axis, forming tunnels along  $[001]$  and  $[110]$  with the  $\text{BiO}_6$  octahedra.<sup>15</sup>

In order to study magnetic, electronic or thermal transport properties in detail at a fundamental level, the use of large high quality single crystals (of either  $\text{Bi}_2\text{CuO}_4$  or  $\text{Bi}_2\text{PdO}_4$ ) is required. Knowledge of the thermodynamic processes and the relevant phase diagrams are essential for crystal growth.

Despite numerous studies on the crystal structure and low temperature magnetic properties of  $\text{Bi}_2\text{CuO}_4$  in the past,<sup>2,8,17–20</sup> there is still no consensus on the  $\text{Bi}_2\text{O}_3$ – $\text{CuO}$

<sup>a</sup> Helmholtz-Zentrum Berlin für Materialien und Energie, Hahn-Meitner-Platz 1, 14109 Berlin, Germany. E-mail: nora.wolff@helmholtz-berlin.de

<sup>b</sup> Leibniz-Institut für Kristallzüchtung, Max-Born-Str. 2, 12489 Berlin, Germany

<sup>c</sup> Institut für Physik und Astronomie, Universität Potsdam, Karl-Liebknecht-Straße 24-25, 14476 Potsdam, Germany

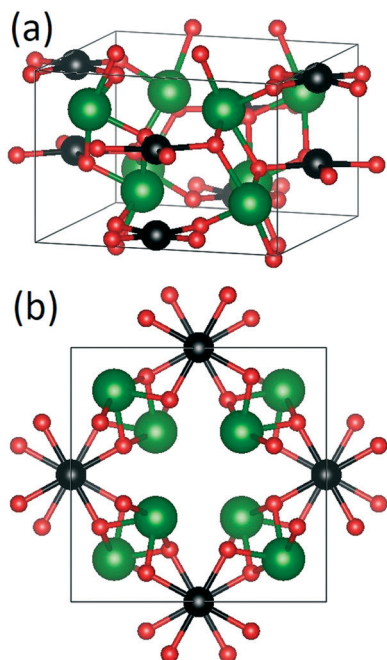



Fig. 1 (a) 3D tetragonal crystal structure of  $\text{Bi}_2\text{MO}_4$  and (b) projection along the  $c$ -axis (green = Bi, black = Cu/Pd, red = O) (drawn with VESTA<sup>30</sup>).

phase diagram and thus the growth conditions required for large, centimeter-sized, high quality  $\text{Bi}_2\text{CuO}_4$  single crystals. In the existing literature, the phase diagrams are very contradictory<sup>21–29</sup> and often the growth conditions are insufficiently detailed.

The phase diagram of  $\text{Bi}_2\text{PdO}_4$  was proposed in 1979 by Kakhan *et al.*<sup>22</sup> and apart from the work by Arpe and Müller-Buschbaum<sup>16</sup> on that system discussing single crystal X-ray diffraction on tiny single crystal samples, to our knowledge no reports on crystal growth of larger single crystals, growth conditions or detailed thermodynamic investigation of  $\text{Bi}_2\text{-PdO}_4$  exist.

The present work therefore focuses on the thermodynamic investigations and the crystal growth of  $\text{Bi}_2\text{M}^{2+}\text{O}_4$  ( $\text{M} = \text{Cu}, \text{Pd}$ ). Phase diagrams that are relevant for the growth of the title compounds are redetermined. We will show that pseudobinary systems of  $\text{Bi}_2\text{O}_3$ – $\text{CuO}$  (– $\text{PdO}$ ) are insufficient to describe the growth process, rather  $\text{Cu}_2\text{O}$  (or  $\text{Pd}$ , respectively) has to be included for a satisfactory description of the experimental results. Redox processes that occur at the phase boundary during melting and crystallization of the  $\text{Bi}_2\text{MO}_4$  phase were investigated. The grown crystals were characterized by powder X-ray diffraction (XRD), Laue, magnetization and specific heat measurements, demonstrating the excellent quality of the crystals synthesized in this work.

## 2 Experimental

### 2.1 Thermodynamics

Investigations on the pseudobinary  $\text{Bi}_2\text{O}_3$ – $\text{CuO}$  and the ternary  $\text{Bi}_2\text{O}_3$ – $\text{Cu}_2\text{O}$ – $\text{CuO}$  phase diagrams are based on powder

mixtures of the raw materials with concentrations between pure  $\text{Bi}_2\text{O}_3$  (Sigma-Aldrich, 5N purity) and 80 mol%  $\text{CuO}$  (Alfa Aesar, 2N7 purity) in  $\text{Bi}_2\text{O}_3$ . Simultaneous thermogravimetric (TG) and differential thermal analysis (DTA) measurements (TG–DTA) were carried out with a Netzsch STA 409C on the powder mixtures placed in  $\text{Al}_2\text{O}_3$  crucibles in air at heating and cooling rates of  $10 \text{ K min}^{-1}$ . In addition, a grown  $\text{Bi}_2\text{CuO}_4$  single crystal was measured using a Netzsch STA 449 F3 with differential scanning calorimetry (DSC–TG) and the sample was placed in a platinum crucible with a lid. For this measurement, an oxygen-enriched atmosphere with flowing 66.7%  $\text{O}_2$  + 33.3% Ar and heating and cooling rates of  $5 \text{ K min}^{-1}$  were used.

The study of the thermodynamic properties of  $\text{Bi}_2\text{PdO}_4$  was carried out on phase pure  $\text{Bi}_2\text{PdO}_4$  powder obtained by the solid state reaction of a mixture in a stoichiometric ratio of  $\text{Bi}_2\text{O}_3$  (Sigma-Aldrich, 5N purity) and  $\text{PdO}$  (Alfa Aesar, 3N purity), sintered three times for 24 h at  $740^\circ\text{C}$  in air with intermediate grindings. Phase purity was confirmed by powder XRD under ambient conditions. TG–DTA measurements were carried out with a Netzsch STA 449 F3 in platinum crucibles at heating and cooling rates of  $10 \text{ K min}^{-1}$ . The gas flow was set using a mass flow controller to deliver atmospheres containing 10%, 20%, 80% and 100%  $\text{O}_2$  in Ar, respectively. The phase composition was additionally studied by means of high temperature XRD measurements performed in air up to  $1000^\circ\text{C}$  using a Bruker D8 Advance diffractometer with  $\text{Cu-K}\alpha$  radiation, equipped with a high temperature oven chamber (Anton Paar HTK 1200 N) and a LynxEye detector for rapid data acquisition.

### 2.2 Crystal growth

In preparation for the crystal growth, polycrystalline rods of  $\text{Bi}_2\text{CuO}_4$  were prepared by mixing  $\text{Bi}_2\text{O}_3$  and  $\text{CuO}$  powders in a 1 : 1 molar ratio followed by sintering in air for 24 h at  $725^\circ\text{C}$ . After this first sintering step, the powder was ground in an agate mortar and sintered again for 24 h at  $750^\circ\text{C}$ . XRD phase analysis confirmed that a single-phase, pure  $\text{Bi}_2\text{CuO}_4$  phase resulted from this annealing process. The sintered material was then reground and compacted in cylindrical rubber balloons and pressed for three minutes at 2 kbar in a cold isostatic press (Engineered Pressure International NV, Belgium). To increase the rod density, the pressed rods were sintered again for 24 h at  $750^\circ\text{C}$ . The final rods were on average about 11 cm long and 6 mm in diameter and had an estimated density of 85% of the theoretical value.

All growth experiments were carried out in an optical floating-zone (OFZ) furnace from Crystal System Corporation (type FZ-T-10000-H-VI-VPO) using polycrystalline feed and seed rods. The furnace consists of a four-mirror setup in which 300 W halogen lamps and a fused silica protection tube were used. For  $\text{Bi}_2\text{CuO}_4$ , an air flow of  $0.3 \text{ l min}^{-1}$  was used as the growth atmosphere, and the  $\text{Bi}_2\text{PdO}_4$  growth experiments were done in a flowing oxygen atmosphere (because the TG measurements in Fig. 5 revealed a significantly stronger tendency to lose oxygen for this compound). Seed and feed rods were rotated in opposite



directions at 30 rpm and at 20 rpm, respectively. To ensure stable growth conditions without cracks, growth rates between 5 and 6 mm h<sup>-1</sup> were employed.

The grown crystals were characterized by XRD and Laue measurements. XRD data on crushed single crystal pieces mixed with a LaB<sub>6</sub> standard were used to determine the lattice parameters of the grown crystals. Magnetization measurements using a Magnetic Property Measurement System (MPMS by Quantum Design Inc.) were carried out between 1.9 K and 350 K on two single crystals with a mass of 40.79 mg and 19.0 mg with a magnetic field applied along the *c* or *a* axis, respectively, for comparison with previously published results and for confirmation of the crystal quality. Low temperature specific heat data between 2 and 100 K were collected in zero field with the standard adiabatic-relaxation technique using the heat capacity option of a Physical Property Measurement System (PPMS by Quantum Design Inc.) on a 7.95 mg sample.

The crystal growth of Bi<sub>2</sub>PdO<sub>4</sub> in the OFZ was also attempted. For this, polycrystalline rods were prepared from a powder mixture of stoichiometric ratios of Bi<sub>2</sub>O<sub>3</sub> and PdO that were sintered 2 times at 740 °C in air with intermediate grindings until a single-phase Bi<sub>2</sub>PdO<sub>4</sub> powder was obtained. The feed and seed rods were then prepared analogously to those of Bi<sub>2</sub>CuO<sub>4</sub> and underwent a final sintering step at 740 °C. The rods were 6 cm long and 6 mm in diameter. The density of the rods was estimated as 75% of the theoretical density, resulting in slightly less compact rods than those of Bi<sub>2</sub>CuO<sub>4</sub>.

## 3 Results and discussion

### 3.1 Thermodynamics

**3.1.1 Bi<sub>2</sub>CuO<sub>4</sub>.** In the past few decades, the system Bi–Cu–O has been investigated several times. Unfortunately, there

are many contradictory phase diagrams for the Bi<sub>2</sub>O<sub>3</sub>–CuO system in the literature,<sup>21–29</sup> and in some references CuBi<sub>4</sub>O<sub>7</sub> is additionally described as an existing phase.<sup>21</sup> In many phase diagrams, the liquidus line is represented as a dashed line due to the reduction process of CuO, which makes it impossible to interpret the measured data clearly.

From our previous investigations on copper oxide compounds, it is known that copper oxide based melts always contain Cu<sup>+</sup> and Cu<sup>2+</sup>.<sup>31–34</sup> Bi<sub>2</sub>CuO<sub>4</sub> contains Cu<sup>2+</sup> which is stabilized by low temperature *T* and high oxygen partial pressure *p*(O<sub>2</sub>) which are the conditions where DTA with powder mixtures of Bi<sub>2</sub>O<sub>3</sub> and CuO was performed. For powders with a CuO concentration of 0 ≤ *x* ≤ 0.5, two endothermal effects with constant onsets at *T*<sub>t</sub> = 732 ± 5 °C and *T*<sub>eut</sub> = 761 ± 5 °C were found, originating from the α–δ transition of Bi<sub>2</sub>O<sub>3</sub> (ref. 35) and the eutectic of Bi<sub>2</sub>O<sub>3</sub> with Bi<sub>2</sub>CuO<sub>4</sub>, respectively. The position of the liquidus could be derived from a bend in the DTA curve only for some samples.

Samples with *x* > 0.45 showed one clear endothermal effect around *T*<sub>per</sub> = 851 ± 10 °C which could be attributed to the (almost, see below) peritectic melting of Bi<sub>2</sub>CuO<sub>4</sub>. However, the width of this DTA peak (Δ*T* ≈ 40 K) did not allow us to discriminate if this effect is really related to peritectic decomposition (like suggested by Hrovat and Kolar<sup>23</sup>) or to congruent melting of Bi<sub>2</sub>CuO<sub>4</sub> with another eutectic towards CuO which is just 5 K below the congruent melting point (like suggested by Kakhan *et al.*<sup>36</sup>).

Despite this ambiguity, these preliminary results allowed successful OFZ growth experiments with 1:1 (molar) Bi<sub>2</sub>O<sub>3</sub>:CuO rods. A small (24.66 mg) Bi<sub>2</sub>CuO<sub>4</sub> single crystal that resulted from the growth experiments was investigated in more sensitive DSC–TG measurements in an atmosphere with a higher oxygen concentration to stabilize Cu<sup>2+</sup>. The results are shown in Fig. 2. During the first heating, the melting peak

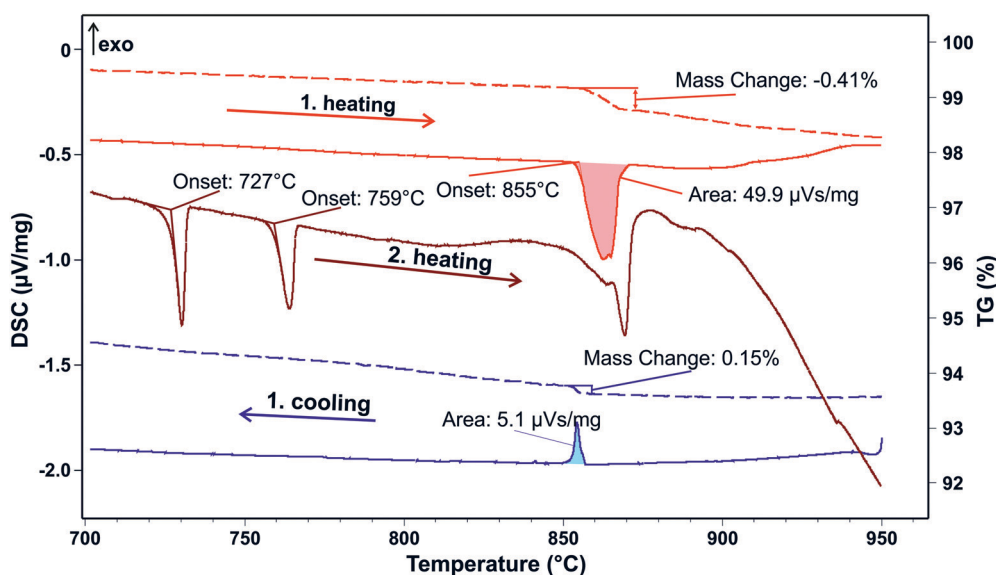


Fig. 2 Bi<sub>2</sub>CuO<sub>4</sub> single crystal TG–DSC measurement (1st and 2nd heating + 1st cooling at 5 K min<sup>-1</sup>) in flowing 66.7% O<sub>2</sub> + 33.3% Ar. Solid lines: DSC, dashed lines: TG.



of the  $\text{Bi}_2\text{CuO}_4$  compound appears at 855 °C and is connected with a mass loss of  $\Delta m/m = -0.41\%$  in the associated TG curve.  $\text{Bi}^{3+}$  can be considered to be stable under the experimental conditions used here. Then, the experimental  $\Delta m/m$  can be attributed to a formal reaction  $\text{Bi}_2\text{CuO}_4 \rightarrow \text{Bi}_2\text{O}_3 + \text{CuO}_{0.86} + 0.07 \text{O}_2$ , because 0.07  $\text{O}_2$  corresponds to a mass loss of 0.41% (some  $\text{Cu}^{2+}$  is reduced to  $\text{Cu}^+$ ). One can assume that  $\text{Cu}^{2+}$  is stabilized in solid  $\text{Bi}_2\text{CuO}_4$  and exists in equilibrium with  $\text{Cu}^+$  in the melt, with a composition that is close to the eutectic composition in the  $\text{Cu}_2\text{O}$ – $\text{CuO}$  system.<sup>37</sup>

This reduction process  $\text{CuO} \rightarrow \text{Cu}_2\text{O}$  continues with further heating, which means that overheating during a crystal growth experiment should be avoided. Experiments in a pure oxygen atmosphere are also not recommended because this increases the liquidus temperature (see Fig. 1 in ref. 37). During the cooling process, the sample gets partially reoxidized ( $\Delta m/m = +0.15\%$ ), connected with an additional small exothermal DTA peak. This is clearly not due to crystallization but results simply from the oxidation  $\text{Cu}_2\text{O} + \frac{1}{2}\text{O}_2 \rightarrow 2\text{CuO}$  with  $\Delta H = -8122 \text{ J per gram O}_2$  (ref. 38) (the sensitivity calibration to convert the peak area of  $5.1 \mu\text{V s mg}^{-1}$  to that enthalpy increment in Fig. 2 was performed at  $T_f = 801 \text{ °C}$  by melting NaCl). Crystallization of the sample occurs with strong supercooling below 700 °C, which is out of the scale of this figure.

Clear evidence for the incongruent nature of melting  $\text{Bi}_2\text{CuO}_4$  is obtained from the second heating of the same sample, which is shown by the middle curve in Fig. 2. The additional peak at  $T_i = 727 \text{ °C}$  results from the  $\alpha$ – $\delta$  transition of  $\text{Bi}_2\text{O}_3$  (ref. 35) and the eutectic of  $\text{Bi}_2\text{O}_3$  with  $\text{Bi}_2\text{CuO}_4$ , as observed in the previous TG–DTA measurements with unreacted powders.

If  $\text{Bi}_2\text{CuO}_4$  were to melt congruently, these two additional peaks would not appear in a second heating run. It should be noted, however, that  $\text{Bi}_2\text{CuO}_4$  is also not melting simply peritectically, because this would imply the formation of a melt under the release of another solid phase (which would be  $\text{CuO}$  here). Here, however, the gas phase is inevitably involved in the melting process.

Data from FactSage<sup>38</sup> databases and from the literature<sup>37,39,40</sup> for  $\text{Bi}_2\text{CuO}_4$  and the  $\text{CuO}_x$ – $\text{Bi}_2\text{O}_3$  melt were refined to describe the experimental data that are reported here, and an isopleth section  $\text{CuO}$ – $\text{Bi}_2\text{O}_3$  of the phase diagram was obtained (Fig. 3). The eutectic point was measured at around 7.5 mol%  $\text{CuO}$  and 761 °C, and is in good agreement with some literature data.<sup>27–29</sup>

Fig. 4 shows the system as a concentration triangle of  $\text{Bi}_2\text{O}_3$ – $\text{Cu}_2\text{O}$ – $\text{CuO}$  at elevated temperatures in air. The red lines show an isothermal section above  $T_{\text{per}} = 857 \text{ °C}$ . On the  $\text{Bi}_2\text{O}_3$ – $\text{CuO}$  side of the phase diagram, only the crystallization phase field of  $\text{CuO}$  is visible. Immediately below the peritectic temperature of 856 °C, the  $\text{Bi}_2\text{CuO}_4$  crystallization phase field begins to expand (the blue phase field in Fig. 4). This field begins slightly above the 0.5 composition of pure  $\text{Bi}_2\text{CuO}_4$ , which indicates the peritectic melting of this phase.

**3.1.2  $\text{Bi}_2\text{PdO}_4$ .** So far, only scarce and contradictory thermodynamic data on the  $\text{Bi}_2\text{O}_3$ – $\text{PdO}$  system can be found in the literature. Hrovat *et al.* reported that  $\text{Bi}_2\text{PdO}_4$  melted incongruently at 845 °C with decomposition into the liquid phase and  $\text{PdO}$ , which in turn dissociates to elemental Pd and oxygen above 800 °C.<sup>41</sup> In contrast, investigations by Kakhan *et al.* revealed congruent melting of  $\text{Bi}_2\text{PdO}_4$  at 855 °C.<sup>22</sup> They report 803 °C as the temperature of the dissociation of  $\text{PdO}$  to Pd metal and oxygen. The melting

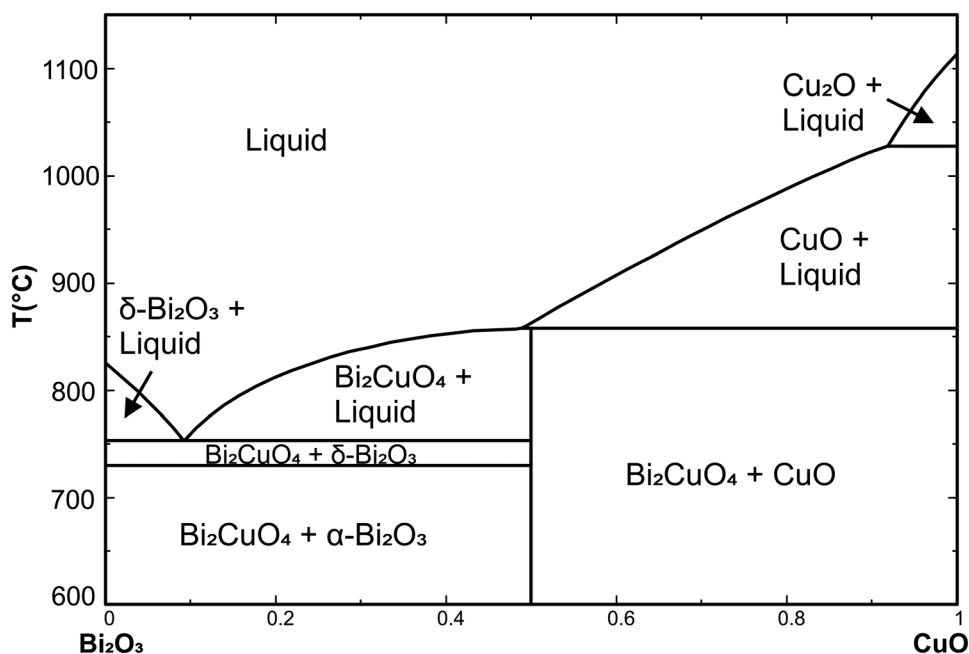


Fig. 3  $\text{Bi}_2\text{O}_3$ – $\text{CuO}$  isopleth section through the system  $\text{Bi}_2\text{O}_3$ – $\text{CuO}$ – $\text{Cu}_2\text{O}$  for  $p(\text{O}_2) = 0.21 \text{ bar}$ .





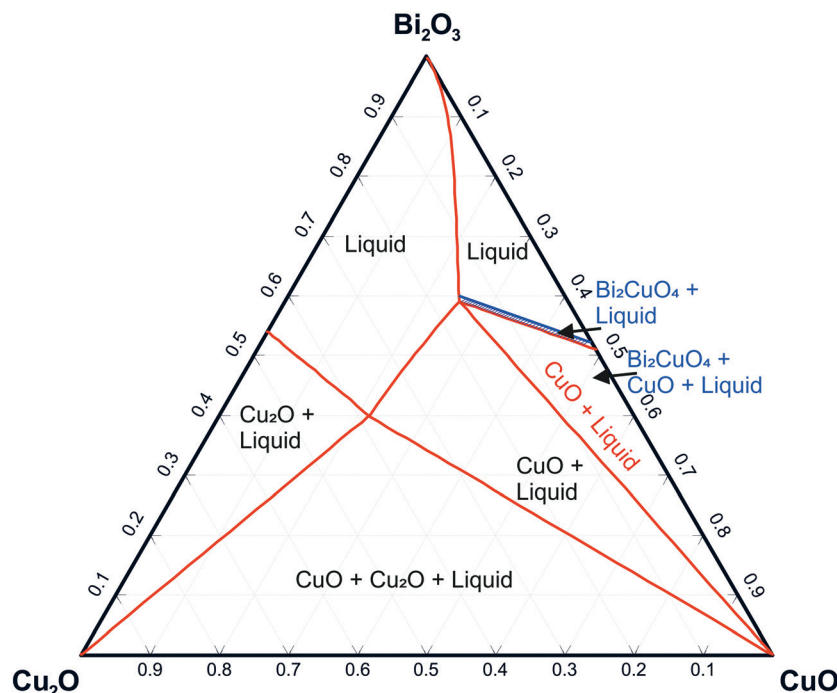


Fig. 4 Isothermal sections through the  $\text{Bi}_2\text{O}_3$ – $\text{Cu}_2\text{O}$ – $\text{CuO}$  system above (857 °C, red) and below (856 °C, blue) the peritectic temperature where  $\text{Bi}_2\text{CuO}_4$  decomposes.

temperatures of  $\text{Bi}_2\text{PdO}_4$  at around 850 °C are in good agreement with our TG-DTA measurement in an atmosphere containing 20%  $\text{O}_2$ , where the onset temperature of the melting peak was defined at 847.7 °C (Fig. 5).

TG-DTA measurements in atmospheres containing between 10 and 100% oxygen revealed that the starting melting process (the onset of DTA curves) is always accompanied by a mass loss. Both effects shift to higher temperatures with increasing  $p(\text{O}_2)$ . For example, at 10%  $\text{O}_2$  ( $p(\text{O}_2) = 0.1$  bar), the melting and immediate  $\text{PdO}$  reduction starts at 826 °C while at 100%  $\text{O}_2$  the reaction starts at 895 °C (Fig. 5). The mass losses are only reversible under sufficiently high  $p(\text{O}_2)$ , *e.g.* under pure  $\text{O}_2$ . Under low  $p(\text{O}_2)$ , the sample mass never returns to the original value, as shown by the red dotted line in Fig. 5.

These observations can be discussed on the basis of the simplified predominance diagram of  $\text{Bi}$ – $\text{Pd}$ – $\text{O}_2$  in Fig. 6 that was calculated with FactSage.<sup>38</sup> Unfortunately, the target phase  $\text{Bi}_2\text{PdO}_4$  itself is not contained in the given databases. To enable its appearance in the diagram, its thermodynamic data were approximated by the sum of the constituents  $\text{Bi}_2\text{O}_3$  and  $\text{PdO}$  (Hess' law), with an additional formation enthalpy of  $-20 \text{ kJ mol}^{-1}$ . Another assumption had to be made regarding the molten phase (liq). For the calculation in Fig. 6, we assumed an ideal miscibility between  $\text{Pd}(\text{liq})$  and  $\text{Bi}_2\text{O}_3(\text{liq})$  because it is well accepted that palladium and silver behave similarly from the chemical point of view<sup>42</sup> and bismuth oxide forms a eutectic with this metal, with a certain degree of miscibility between the liquid metal and oxide.<sup>43</sup>

The diagram shows that under the given experimental conditions, bismuth always exists as  $\text{Bi}^{3+}$ . Palladium, in contrast, can exist as  $\text{Pd}^{4+}$ ,  $\text{Pd}^{2+}$ , or as metallic  $\text{Pd}^0$ . The formation of  $\text{Bi}_2\text{PdO}_4$  stabilizes the divalent  $\text{Pd}^{2+}$  and free  $\text{PdO}$  does not appear in the predominance diagram because it dissociates above 800 °C.<sup>44</sup> This also explains the observed mass loss during melting. A peritectic melting process  $\text{Bi}_2\text{PdO}_4 \rightarrow \text{PdO} + \text{liq}$  would lead to a  $\text{Bi}_2\text{O}_3$ -rich melt under the release of solid  $\text{PdO}$ . In contrast, the melting observed here is described by the reaction  $\text{Bi}_2\text{PdO}_4 \rightarrow \text{Pd} + \frac{1}{2}\text{O}_2 + \text{liq}$ . This latter reaction cannot be reversed as easily as the first one because it requires the uptake of free oxygen from the atmosphere. Obviously, this is only possible in very oxygen rich atmospheres, but not for 10%  $\text{O}_2$  in Ar as shown in Fig. 5 for the blue and red dotted lines, respectively. In particular, the loss of one oxygen atom per formula unit of  $\text{Bi}_2\text{PdO}_4$  *via*  $\text{PdO} \rightarrow \text{Pd} + \frac{1}{2}\text{O}_2$  would result in a theoretical mass loss of 2.7% which is in good agreement with the TG curves in Fig. 5.

The stability of the phases in the system  $\text{Bi}$ – $\text{Pd}$ – $\text{O}_2$  as a function of the oxygen partial pressure and temperature can be qualitatively described in the predominance diagram as shown in Fig. 6. The vertical lines depict the different melting processes and the phase transition of  $\text{Bi}_2\text{O}_3$  at 730 °C. In particular, the previously discussed melting of  $\text{Bi}_2\text{PdO}_4$  corresponds to the phase boundary  $\text{Bi}_2\text{PdO}_4/\text{liq} + \text{Pd}$ .

High temperature XRD measurements revealed the presence of elemental  $\text{Pd}$  in the melt above 860 °C which does not dissolve even at higher temperatures. This



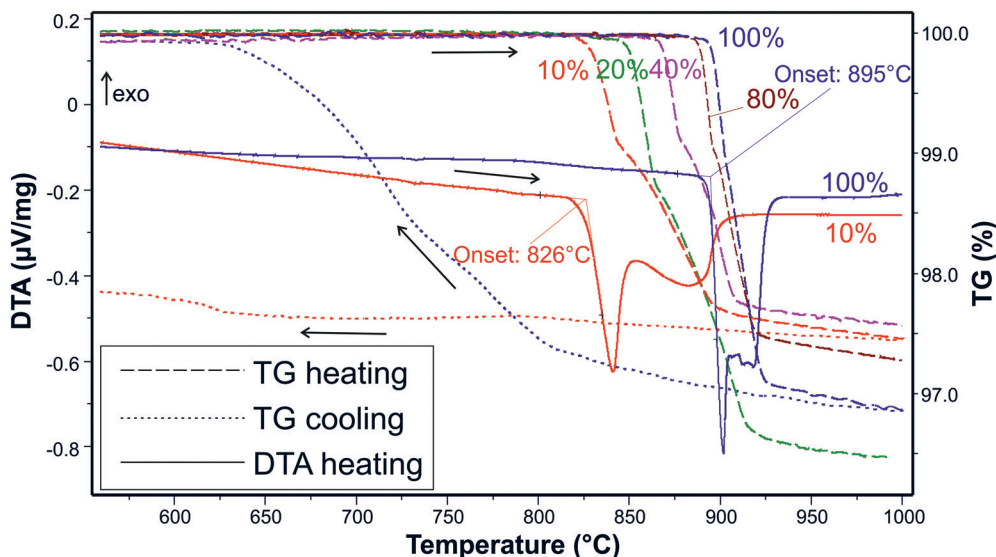


Fig. 5 TG heating curves of  $\text{Bi}_2\text{PdO}_4$  in five different atmospheres from 100%  $\text{O}_2$  to 10%  $\text{O}_2$  in Ar ( $\text{O}_2$  concentration given as a parameter). For the measurements at 100% (blue) and 10%  $\text{O}_2$  (red), DTA heating and TG cooling curves are shown additionally.

elemental Pd makes the crystal growth method used in this work unsuitable, since Pd interferes in the melt zone. Alternative growth methods using a crucible could be advantageous for  $\text{Bi}_2\text{PdO}_4$  but further research needs to be done on this.

For stable growth, it is crucial that the elemental Pd is reoxidized during crystallization. Our TG–DTA measurements showed that at least 80%  $\text{O}_2$  in the atmosphere is necessary to achieve complete reoxidation.

Typical binary  $\text{Bi}_2\text{O}_3$ –PdO phase diagrams from the literature<sup>41,22</sup> must be used with caution because PdO is actually reduced, and is hence not a valid component of the system. Our TG–DTA measurements show that additional

melting peaks in a second heating cycle occur even in 100%  $\text{O}_2$  (not shown in Fig. 5), irrespective of Pd seemingly being reoxidized during the first cooling. These additional peaks can be assigned to the  $\text{Bi}_2\text{O}_3$  phase transition and the eutectic line, which in turn implies the peritectic melting of the  $\text{Bi}_2\text{PdO}_4$  phase. However, the melting of  $\text{Bi}_2\text{PdO}_4$  can only be viewed correctly in the Bi–Pd–O ternary system, since the melting and crystallization are connected to redox processes. It should be noted that the ternary system depends strongly on the atmospheric conditions. A complete thermodynamic assessment of this ternary system, which would adjust Fig. 6 quantitatively to the experimental data, is beyond the scope of this paper.

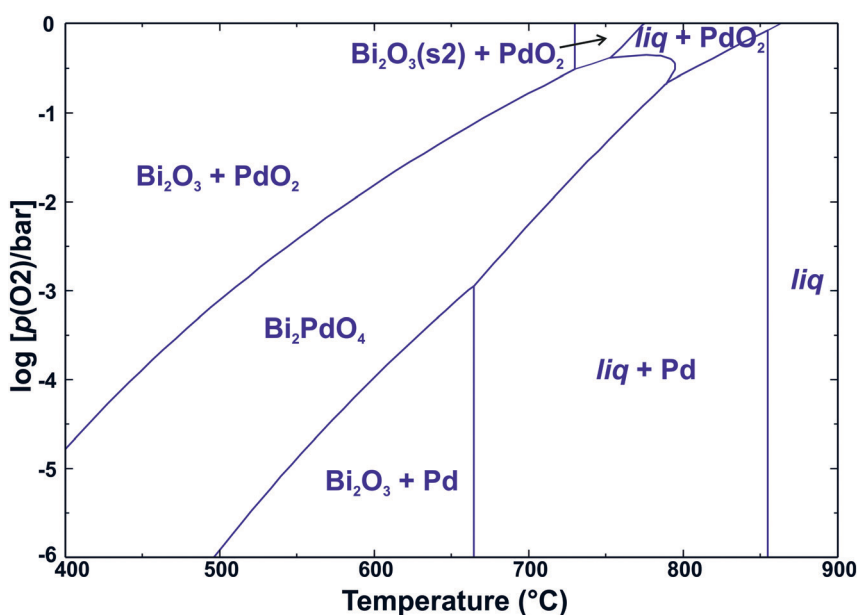
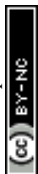


Fig. 6 Phase stability in the system Bi–Pd– $\text{O}_2$ . An enthalpy of 20  $\text{kJ mol}^{-1}$  was assumed for the reaction  $\text{Bi}_2\text{O}_3 + \text{PdO} \rightarrow \text{Bi}_2\text{PdO}_4$ .



### 3.2 Crystal growth

The growth of  $\text{Bi}_2\text{CuO}_4$  single crystals was performed by taking into account the results of our above-described thermodynamic investigations. Even though  $\text{Bi}_2\text{CuO}_4$  melts incongruently (Fig. 3), higher growth rates (up to  $6 \text{ mm h}^{-1}$ ) than usually possible with incongruently melting compounds can be used. This is probably enabled by the strong tendency of the melt to supercooling, allowing crystal growth below the equilibrium melting temperature from a stoichiometric equimolar melt. XRD measurements of the initially crystallized material revealed that indeed not  $\text{CuO}_x$  but  $\text{Bi}_2\text{CuO}_4$  is formed. The growth of  $\text{Bi}_2\text{CuO}_4$  from a stoichiometric melt is supported because it melts only slightly peritectically. It should be noted that in some other systems even Czochralski crystal growth proved to be possible significantly below the equilibrium melting point. Kouta *et al.* demonstrated the growth of  $\beta\text{-BaB}_2\text{O}_4$  (stable below  $920^\circ\text{C}$ ) from a stoichiometric melt that is in equilibrium with the high-temperature  $\alpha\text{-BaB}_2\text{O}_4$  at  $1095^\circ\text{C}$ ,  $175 \text{ K}$  above that of the  $\alpha\text{-}\beta$  transition.<sup>45</sup>

A growth rate of  $>5.5 \text{ mm h}^{-1}$  leads to a stable growth, and less cracks occur. So far, there are only a few publications on the crystal growth of  $\text{Bi}_2\text{CuO}_4$  and in most works lower (typically  $3$  or  $5 \text{ mm h}^{-1}$  (ref. 8, 46)) or higher ( $10 \text{ mm h}^{-1}$  (ref. 8, 46–48)) growth rates were used, which could be a reason for cracking. It is also described that a growth rate of  $10 \text{ mm h}^{-1}$  improves the growth process because the low surface tension of the melt is problematic, but the crystal quality is lower.<sup>8,46</sup> In some experiments, excess  $\text{CuO}$ <sup>46</sup> or a pure oxygen atmosphere<sup>8</sup> was used, which is, as described in our Thermodynamics section, not advantageous for the growth. The experiments in this work showed that the growth is most stable and crack-free crystals are obtained at a rate of  $6 \text{ mm h}^{-1}$ . When using polycrystalline seeds, however, the first grown  $15\text{--}20 \text{ mm}$  are always completely covered with cracks.

Although a growth rate of  $6 \text{ mm h}^{-1}$  leads to crack-free growth, the  $\text{CuO}_x$  equilibrium in the melt cannot adjust fast enough. During the growth,  $\text{CuO}$  is removed from the melt, which leads to an increase in the  $\text{Cu}_2\text{O}/\text{CuO}$  ratio. This in turn leads to an increase in the liquidus temperature (see Fig. 1 in ref. 37). Therefore, the lamp power must be adjusted continuously, even if only in very small steps, during the growth experiments. The typical power of  $300 \text{ W}$  lamps during an experiment was, for example, between  $30.80\text{--}31.67\%$ .

Taking into account the thermodynamic investigations of this work and based on the chosen growth parameters and instrumental conditions, it was possible to grow  $\text{Bi}_2\text{CuO}_4$  crystals with lengths of up to  $7 \text{ cm}$  and diameters of  $6 \text{ mm}$  (Fig. 7). The crystals show a rough surface in the later stages of the growth which is probably related to  $\text{Cu}_2\text{O}$  deposition. However, a clear proof of this assumption could not be provided by XRD and XRF measurements. Laue measurements along the crystal length show a constant

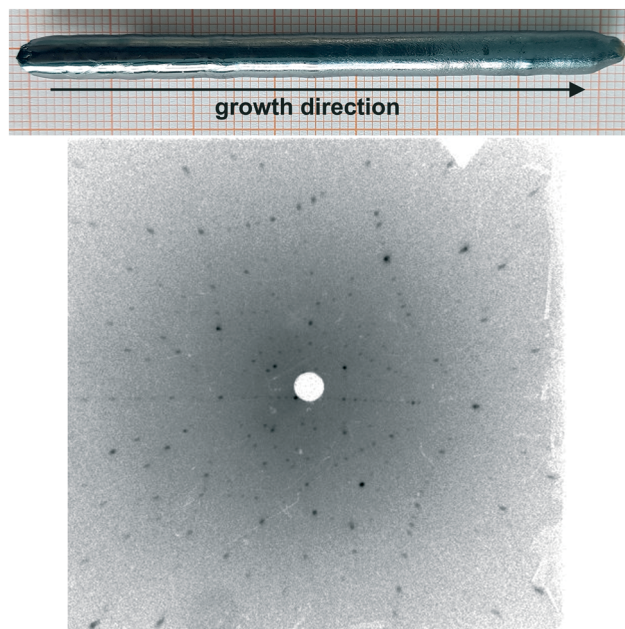


Fig. 7  $\text{Bi}_2\text{CuO}_4$  single crystal with excess copper oxide on the surface in the later stages of the growth (top) and Laue measurement confirming the  $[120]$  growth direction (bottom).

orientation, which proves that the grown materials are single crystalline. The preferred growth direction of the crystals is along  $[120]$  (Fig. 7), but this is only the case in 3 of 4 grown crystals, and the cleavage is typically along  $(001)$ , since the interatomic distances are larger in this direction, resulting in a weaker bond.<sup>18</sup> The lattice parameters were refined using powder X-ray diffraction data on crushed single crystal pieces. It was found that  $\text{Bi}_2\text{CuO}_4$  crystallizes in the tetragonal space group  $P4/ncc$  (130) with the lattice constants  $a = 8.501(1) \text{ \AA}$  and  $c = 5.818(4) \text{ \AA}$ , which are in good agreement with the crystal refinement by Yamada *et al.*<sup>18</sup>

Magnetic susceptibility  $\chi = M/H$  and specific heat data on the single crystal samples of  $\text{Bi}_2\text{CuO}_4$  as a function of temperature are shown in Fig. 8. In agreement with earlier studies,<sup>8,18,49,50</sup> the temperature dependence of the susceptibility upon cooling is characterized by an increase of  $\chi(T)$  leading to a broad hump with a maximum in  $\chi(T)$  at  $\sim 50 \text{ K}$ , followed by an abrupt drop at around  $43.8 \text{ K}$  signaling the onset of the long-range antiferromagnetic order at that temperature (*i.e.* the Néel temperature,  $T_N$ ), and by a further decrease before an upturn below about  $25 \text{ K}$ . The emergence of the long-range antiferromagnetic order at  $T_N \sim 43.8 \text{ K}$  is further corroborated by the sharp  $\lambda$ -like anomaly in the specific heat (Fig. 8 inset) obtained in zero field. The magnetic susceptibility is, also consistent with earlier reports,<sup>8,18,50</sup> anisotropic with a larger susceptibility along the  $c$  axis than along directions perpendicular to it, and it is highly field-dependent for applied fields of  $<1 \text{ T}$  along the  $a$  axis below  $T_N$  (not shown here). Our magnetization and specific heat data therefore show that our  $\text{Bi}_2\text{CuO}_4$  single crystals are of high crystalline quality.





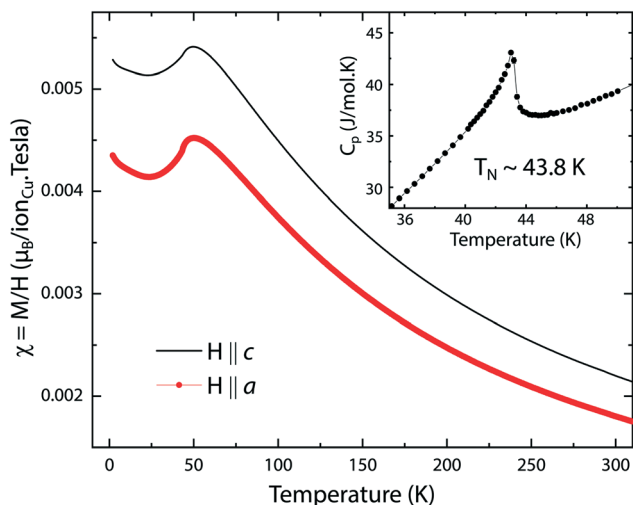


Fig. 8 Temperature dependence of the magnetic susceptibility  $\chi(T)$  in a magnetic field of 1 T applied along two perpendicular directions, along the  $c$  and  $a$  axes in  $\text{Bi}_2\text{CuO}_4$ , respectively. The inset shows the  $a$ -like specific heat anomaly associated with the antiferromagnetic ordering at  $T_N \sim 43.8$  K.

It was not possible to grow  $\text{Bi}_2\text{PdO}_4$  crystals by the OFZ technique, because the elemental Pd prevents the formation of a melt zone (as discussed in the Thermodynamics section).

## 4 Summary and conclusions

Phase equilibria that are relevant for the growth of the title compounds were studied experimentally, and a semiquantitative description in terms of the ternary systems  $\text{Bi}_2\text{O}_3\text{--CuO--Cu}_2\text{O}$  or  $\text{Bi}_2\text{O}_3\text{--PdO}_2\text{--Pd}$ , respectively, was given. High-quality  $\text{Bi}_2\text{CuO}_4$  single crystals with lengths of up to 7 cm and diameters of 6 mm were grown by the OFZ technique. Based on the results of the Laue, magnetization and specific heat measurements, we confirm the excellent quality of our grown samples. The growth of  $\text{Bi}_2\text{PdO}_4$  by the OFZ technique is precluded, since the elemental Pd prevents the formation of a melt zone and other techniques such as the Czochralski method should be used for the growth of this material.

It could be shown that pseudobinary systems of  $\text{Bi}_2\text{O}_3\text{--CuO}$  ( $\text{--PdO}$ ) are insufficient to describe the growth process, because every crystallization or melting process of the  $\text{Bi}_2\text{M}^{2+}\text{O}_4$  phase is accompanied by a redox process that can only be accounted for in the ternary systems. The melting processes of  $\text{Bi}_2\text{CuO}_4$  and  $\text{Bi}_2\text{PdO}_4$  are often called “peritectic”, which is not totally true: a peritectic reaction follows the scheme solid (1)  $\rightarrow$  solid (2) + melt. In contrast, the melting/crystallization of the compounds in this study has the scheme  $\text{Bi}_2\text{CuO}_4 \rightleftharpoons \text{CuO} + (\text{Bi}_2\text{O}_3 + \text{CuO}_x)$  melt +  $\text{O}_2$  or  $\text{Bi}_2\text{PdO}_4 \rightleftharpoons \text{Pd} + (\text{Bi}_2\text{O}_3 + \text{Pd})$  melt +  $\text{O}_2$  under the involvement of the gas phase. We recommend for this type of melting the term “exaperitectic” (greek:  $\epsilon\zeta\alpha\rho\mu\iota\sigma\eta$  = to exhaust).

For both title compounds, the valence state of the transition metal is lowered during melting ( $\text{Cu}^{2+} \rightarrow \text{Cu}^{2+} +$

$\text{Cu}^+$  or  $\text{Pd}^{2+} \rightarrow \text{Pd}^0$ ) under the release of free oxygen. Consequently,  $\text{O}_2$  must be transported through the melt to the phase boundary during the crystal growth process to ensure the crystallization of high-quality stoichiometric  $\text{Bi}_2\text{CuO}_4$  and  $\text{Bi}_2\text{PdO}_4$ . This is a process that limits the growth rate. When using a growth rate of  $6 \text{ mm h}^{-1}$ , as in the case of our  $\text{Bi}_2\text{CuO}_4$  growth experiments, the  $\text{CuO}_x$  equilibrium in the melt cannot adjust fast enough, which leads to an increase of the liquidus temperature. During this growth process, the lamp power needs to be adjusted continuously. In the case of  $\text{Bi}_2\text{PdO}_4$ , other growth techniques are recommended, as the reoxidation of the elemental Pd needs more time and besides the formation of a melt zone is prevented.

## Conflicts of interest

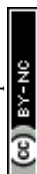
The authors declare no conflict of interest.

## Acknowledgements

The use of HZB's X-ray Corelab and the Corelab for Quantum Materials is acknowledged. We thank R. Gunder, K. Siemensmeyer and R. Feyerherm for technical support and N. Islam and K. Karmakar for helpful discussions on the OFZ setup. J.-E. Hoffmann is thanked for technical support with the TG-DTA setup.

## References

- 1 M. A. Hayward, *Inorg. Chem.*, 2019, **58**, 11961–11970.
- 2 J. L. Garcia-Munoz, J. Rodriguez-Carvajal, F. Sapina, M. J. Sanchis, R. Ibanez and D. Beltran-Porter, *J. Phys.: Condens. Matter*, 1990, **2**, 2205–2214.
- 3 S. Kanungo, B. Yan, P. Merz, C. Felser and M. Jansen, *Angew. Chem., Int. Ed.*, 2015, **54**, 1–5.
- 4 K. Yoshii, T. Fukuda, H. Akahama, J. Kano, T. Kambe and N. Ikeda, *Phys. C*, 2011, **471**, 766–769.
- 5 Z. V. Popovic, G. Kliche, M. J. Konstantinovic and A. Revcolevschi, *J. Phys.: Condens. Matter*, 1992, **2**, 10085–10092.
- 6 L. E. Svistov, V. A. Chubarenko, A. Y. Shapiro, A. V. Zaleskii and G. A. Petrakovskii, *J. Exp. Theor. Phys.*, 1998, **86**, 1228–1233.
- 7 B. Yuan, N. P. Butch, G. Xu and Y.-J. Kim, 2019, *arXiv*, 1907.07784, pp. 2406–2414.
- 8 L. Zhao, H. Guo, W. Schmidt, K. Nemkovski, M. Mostovoy and A. C. Komarek, *Phys. Rev. B*, 2017, **96**, 054424.
- 9 D. Di Sante, P. Hausoel, A. Barone, J. M. Tomczak, G. Sangiovanni and R. Thomale, *Phys. Rev. B*, 2017, **96**, 121106.
- 10 S. P. Berglund, F. F. Abdi, A. Bogdanoff, P. Chemseddine, D. Friedrich and R. van de Krol, *Chem. Mater.*, 2016, **28**, 4231–4242.
- 11 N. Xu, F. Li, L. Gao, H. Hu, Y. Hu, X. Long, J. Ma and J. Jin, *ACS Sustainable Chem. Eng.*, 2018, **6**, 7257–7264.
- 12 Y.-H. Choi, D.-H. Kim and S.-H. Hong, *ACS Appl. Mater. Interfaces*, 2018, **10**, 14901–14913.





- 13 L. K. Lamontagne, G. Laurita, M. W. Gaultois, M. Knight, L. Ghadbeigi, T. D. Sparks, M. E. Gruner, R. Pentcheva, C. M. Brown and R. Seshadri, *Chem. Mater.*, 2016, **28**, 3367–3373.
- 14 T. C. Ozawa, T. Taniguchi, Y. Nagata, Y. Noro, T. Naka and A. Masushita, *J. Alloys Compd.*, 2005, **388**, 1–5.
- 15 J. He, S. Hao, Y. Xia, S. S. Naghavi, V. Ozolins and C. Wolverton, *Chem. Mater.*, 2017, **29**, 2529–2534.
- 16 R. Arpe and H. Müller-Buschbaum, *Z. Naturforsch.*, 1976, **31b**, 1708–1709.
- 17 J. P. Attfield, *J. Phys.: Condens. Matter*, 1989, **1**, 7045.
- 18 K. Yamada, K. Takada, S. Hosoya, Y. Watanabe, Y. Endoh, N. Tomonaga, T. Suzuki, T. Ishigaki, T. Kamiyama, H. Asano and F. Izumi, *J. Phys. Soc. Jpn.*, 1991, **60**, 2406–2414.
- 19 K. Sreedhar, *J. Phys. C: Solid State Phys.*, 1129, **21**, 1129.
- 20 R. Troc, J. Janicki, I. Filatow, P. Fischer and A. Murasik, *J. Phys.: Condens. Matter*, 1990, **2**, 6989–6998.
- 21 J. Cassedanne and C. P. Campelo, *An. Acad. Bras. Cienc.*, 1966, **38**, 35–38.
- 22 B. G. Kakhan, V. B. Lazarev and I. S. Shaplygin, *Zh. Neorgan. Khim.*, 1979, **24**, 1663–1668.
- 23 M. Hrovat and D. Kolar, *J. Mater. Sci. Lett.*, 1984, **3**, 659–662.
- 24 J. C. Boivin, D. J. Thomas and G. Tridot, *C. R. Seances Acad. Sci., Ser. C*, 1973, **276**, 1105–1107.
- 25 Z. K. Huang, Y. X. Jia, J. X. Chen, P. L. Wang, R. F. Huang and D. S. Yan, *Wuji Cailiao Xuebao*, 1990, **5**, 375–376.
- 26 M. P. Kulakov and D. Y. Lenchienko, *Thermochim. Acta*, 1991, **188**, 129–133.
- 27 M. Nevriiva, H. Kraus and D. Sedmidubsky, *Thermochim. Acta*, 1996, **282/283**, 205–224.
- 28 J. Sestak, D. Sedmidubsky and G. K. Moiseev, *J. Therm. Anal.*, 1997, **48**, 1105–1122.
- 29 B. Hallstedt, D. Risold and L. J. Gauckler, *J. Am. Ceram. Soc.*, 1996, **79**, 353–358.
- 30 K. Momma and F. Izumi, *J. Appl. Crystallogr.*, 2011, **44**, 1272–1276.
- 31 N. Wolff, D. Klimm and D. Siche, *J. Solid State Chem.*, 2018, **258**, 495–500.
- 32 N. Wolff, D. Klimm, S. Ganschow and D. Siche, *Cryst. Res. Technol.*, 2019, **54**, 1900036.
- 33 N. Wolff, *PhD thesis*, Technische Universität Berlin, Germany, 2019.
- 34 N. Wolff, T. Schwaigert, D. Siche, D. G. Schlom and D. Klimm, *J. Cryst. Growth*, 2020, **532**, 125426.
- 35 F. Schröder, N. Bagdassarov, F. Ritter and L. Bayarjargal, *Phase Transitions*, 2010, **83**, 311–325.
- 36 B. G. Kakhan, V. B. Lazarev and I. S. Shaplygin, *Zh. Neorg. Khim.*, 1979, **24**, 1663–1668.
- 37 L. Schramm, G. Behr, W. Löser and K. Wetzig, *J. Phase Equilib. Diffus.*, 2005, **26**, 605–612.
- 38 *FactSage 7.3*, GTT Technologies, Kaiserstr. 100, 52134 Herzogenrath, Germany, 2019, www.factsage.com.
- 39 A. Strejc, D. Sedmidubský, K. Růžicka and J. Leitner, *Thermochim. Acta*, 2003, **402**, 69–74.
- 40 V. M. Denisov, L. A. Irtyugo, L. T. Denisova, S. D. Kirik and L. G. Chumilina, *Phys. Solid State*, 2012, **54**, 1943–1945.
- 41 M. Hrovat, S. Bernik and D. Kolar, *J. Mater. Sci. Lett.*, 1988, **7**, 637–638.
- 42 A. G. Massey, N. R. Thompson and B. F. G. Johnson, *The Chemistry of Copper, Silver and Gold*, Pergamon, 1973, p. 93.
- 43 J. Assal, B. Hallstedt and L. J. Gauckler, *J. Am. Ceram. Soc.*, 1999, **82**, 711–715.
- 44 G. Bayer and H. Wiedemann, *Thermochim. Acta*, 1975, **11**, 79–88.
- 45 H. Kouta, Y. Kuwano, K. Ito and F. Marumo, *J. Cryst. Growth*, 1991, **114**, 676–682.
- 46 B. D. White, W. M. Pätzold and J. J. Neumeier, *Phys. Rev. B: Condens. Matter Mater. Phys.*, 2010, **82**, 094439.
- 47 M. J. Konstantinovic, Z. V. Popovic, S. D. Devic, A. Revcolevschi and G. Dhalenne, *J. Phys.: Condens. Matter*, 1992, **4**, 7913–7918.
- 48 G. Dhalenne, A. Revcolevschi, M. Ain, B. Hennion, G. Andre and G. Parette, *Cryst. Prop. Prep.*, 1991, **36–38**, 11–16.
- 49 M. Baran, Y. Gaidukov, N. Danilova, A. Inushkin, A. Jedrzejczak, Y. Koksharov, V. Nikiforov, A. Revcolevschi, R. Szymczak and H. Szymczak, *J. Magn. Magn. Mater.*, 1999, **196–197**, 532–533.
- 50 M. Herak, M. Miljak, G. Dhalenne and A. Revcolevschi, *J. Phys.: Condens. Matter*, 2009, **22**, 026006.

